Electrolytic Reduction of Solid AlO to Liquid Al in Molten CaCl

AUTHOR(S):

Kadowaki, Haruna; Katasho, Yumi; Yasuda, Kouji; Nohira, Toshiyuki

CITATION:

Kadowaki, Haruna ...[et al]. Electrolytic Reduction of Solid AlO to Liquid Al in Molten CaCl. JOURNAL OF THE ELECTROCHEMICAL SOCIETY 2018, 165(2): D83-D89

ISSUE DATE:

2018

URL:

http://hdl.handle.net/2433/234817

Electrolytic Reduction of Solid Al_2O_3 to Liquid Al in Molten $CaCl_2$

Haruna Kadowaki,[1] Yumi Katasho,[1] Kouji Yasuda,[2,3,*] and Toshiyuki Nohira [1,*,z]

[1] *Institute of Advanced Energy, Kyoto University, Gokasho, Uji, Kyoto 611-0011, Japan*
[2] *Agency for Health, Safety and Environment, Kyoto University, Yoshida-Hommachi, Sakyo-ku, Kyoto 606-8501, Japan*
[3] *Graduate School of Energy Science, Kyoto University, Yoshida-Hommachi, Sakyo-ku, Kyoto 606-8501, Japan*

The electrochemical reduction of Al_2O_3 has been investigated in molten $CaCl_2$ at 1123 K. To predict the electrochemical reduction behavior depending on the activity of O^{2-} ions, the potential–pO^{2-} diagram for the Al–Ca–O–Cl system is constructed from thermochemical data. In a Mo box-type electrode, an Al_2O_3 tube is successfully reduced to liquid Al with a maximum purity of 98 at%. However, in the electrolysis of Al_2O_3 powder in an Fe box-type electrode, Al_2Ca is produced through the formation of $Ca_{12}Al_{14}O_{33}$ as an intermediate product. The different electrochemical reduction behaviors of the tube and the powder are explained by the different diffusion path lengths for O^{2-} ions from three-phase zone (Al_2O_3/$CaCl_2$/cathode metal) to bulk $CaCl_2$.
 [DOI: 10.1149/2.1191802jes]

Manuscript submitted November 13, 2017; revised manuscript received January 15, 2018. Published January 30, 2018.

Aluminum metal is conventionally produced by the electrolytic reduction of Al_2O_3 in high-temperature fluoride-based molten salts, which is known as the Hall–Héroult process. The aluminum industry has remarkably advanced since the invention of this process in 1886. However, this process still consumes a large amount of electric power. Additionally, the generation of large amounts of CO_2 and small amounts of perfluorocarbon gases at the anode causes global warming. Therefore, it is essential to develop an environmentally friendly production process of aluminum.

Meanwhile, electrolytic reductions of various kinds of solid oxides in $CaCl_2$ and/or $CaCl_2$-based molten salts have been investigated by many researchers in the last two decades.[1–17] Fray et al. reported the direct electrolytic reduction of TiO_2 pellets in a $CaCl_2$-based melt, known as the FFC Cambridge process.[1–6] This process has the potential to replace the conventional Kroll process for producing Ti metal, owing to its simple system and relatively low temperature. The direct electrolytic reduction of SiO_2 in molten $CaCl_2$ at 1123 K was first reported by our group by using SiO_2 contacting electrodes.[7] To date, many studies aimed at the production of SOG-silicon and other materials[8–12] have been conducted. In the electrolytic reduction of SiO_2 granules in molten $CaCl_2$ at 1123 K,[12] the current density was comparable to that in the commercial Hall–Héroult process.

For the electrochemical reduction of Al_2O_3, there have been several studies conducted in $CaCl_2$-based melts.[13–17] Yan investigated the reduction of Al_2O_3 tube using a Nb box-type cathode in molten $CaCl_2$–NaCl at 1173 K.[13] In this study, Al-rich Al–Ca alloy droplets with 84.9–98.4 at%Al was obtained. Yan and Fray also reported the electrochemical reduction of Al_2O_3 in $CaCl_2$–LiCl at 973 K and $CaCl_2$–NaCl at 1173 K.[15] They reported that calcium aluminate was formed as an intermediate product during the electrolysis. Xie et al.[14,16] also reported that Al droplets were obtained by the electrochemical reduction of Al_2O_3 in molten $CaCl_2$–NaCl at 823 K[14] and at 1073 K.[16] However, the purity of Al droplets was not clear. In all above studies, because they used a two-electrode system, the reaction mechanism, including the relations between the electrode potential and the formation phase, has not been clarified yet. Recently, Suzdaltev et al. reported that Al_2O_3 powder was chemically reduced by electrochemically produced Ca^+ and Ca in $CaCl_2$–CaF_2 melt at 1023 K.[17] However, the role and influence of F^- ions, such as in the dissolution of Al_2O_3 to the melt, has not been understood well and the obtained Al droplets contained Al–Ca alloys. Despite the extensive studies, the electrochemical reduction behavior of Al_2O_3 in pure molten $CaCl_2$ has not been identified.

In the present study, we have selected $CaCl_2$ as a molten salt, owing to its many desirable properties: high solubility of O^{2-} ions,[18] low cost, and no emission of fluorocarbon gases. Compared with $CaCl_2$–NaCl and $CaCl_2$–KCl, pure $CaCl_2$ has higher solubility of O^{2-} ions, which is kinetically advantageous for the electrochemical reduction of metal oxides. When carbon is used as an anode, the expected reactions for the production of Al metal from Al_2O_3 in molten $CaCl_2$ are:

$$\text{Cathodic reaction:} \quad Al_2O_3\,(s) + 6\,e^- \rightarrow 2\,Al\,(l) + 3\,O^{2-}, \qquad [1]$$

$$\text{Anodic reaction:} \quad C\,(s) + xO^{2-} \rightarrow CO_x\,(g) + 2xe^-. \qquad [2]$$

A conceptual drawing of the electrolytic cell for the reduction of Al_2O_3 powder proposed in this study is shown in Fig. 1. In a semi-continuous process, similar to the Hall–Héroult process, the charging of Al_2O_3 powder from the top of the cell and recovery of liquid Al metal produced at the bottom cathode, are realized. The density of Al_2O_3, $CaCl_2$, and Al are 3.95 g cm^{-3}, 2.09 g cm^{-3}, and 2.38 g cm^{-3} at 1123 K, respectively. Although the density of Al_2O_3 is larger than Al, powdery Al_2O_3 is expected to float on the liquid Al due to the low wettability between Al and Al_2O_3.[19]

To develop the alternative process of Al production, we report the following thermodynamic considerations and fundamental experimental results. First, the potential–pO^{2-} diagrams for the Al–Ca–O–Cl system in molten $CaCl_2$ at 1123 K are constructed from

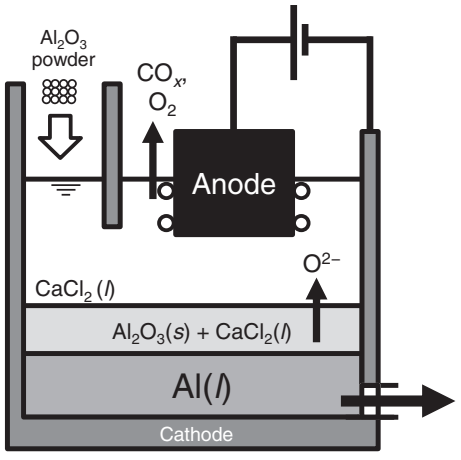

Figure 1. Conceptual drawing of the electrolytic cell for the reduction of Al_2O_3 powder. Al_2O_3 powder is charged from the top of the cell and reduced to Al at the bottom.

*Electrochemical Society Member.
zE-mail: t-nohira@iae.kyoto-u.ac.jp

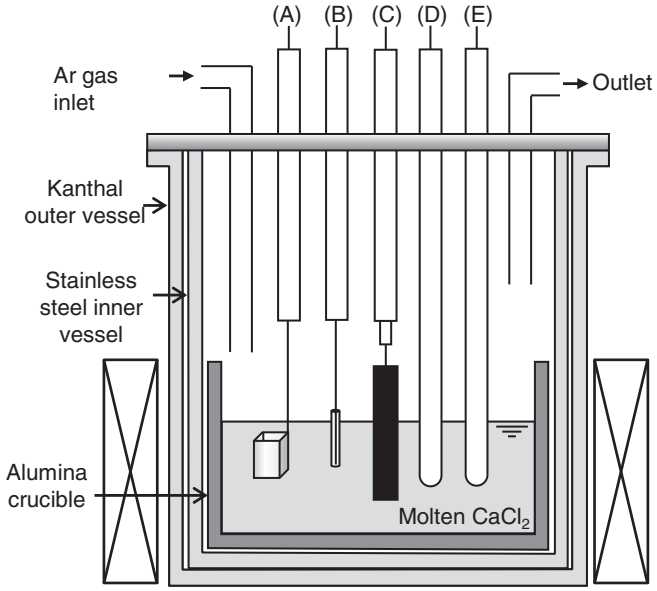

Figure 2. Schematic figure showing the experimental apparatus. (A) Working electrode (box electrode), (B) working electrode (Al_2O_3-sealed electrode), (C) graphite counter electrode, (D) Ag^+/Ag reference electrode, and (E) thermocouple.

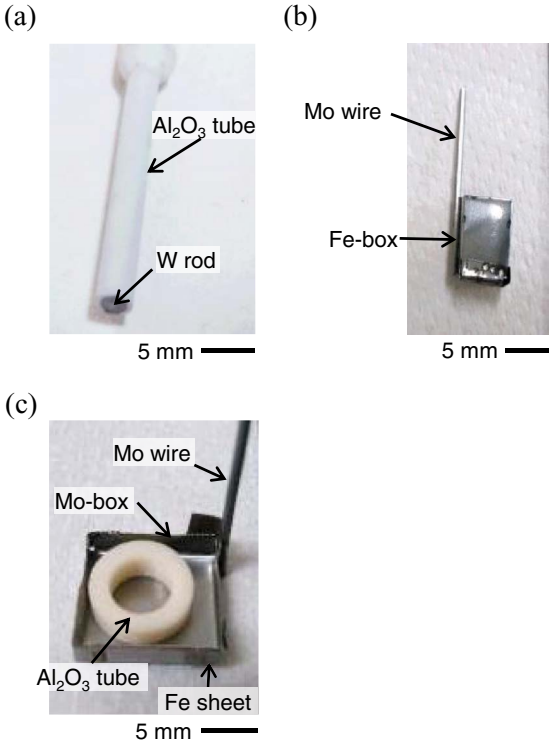

Figure 3. Photographs of the Al_2O_3 contacting electrodes. (a) Al_2O_3-sealed electrode, (b) Fe-box electrode (Al_2O_3 powder was contained), and (c) Mo-box electrode (Al_2O_3 tube was placed).

thermochemical data to predict and discuss the reaction products depending on activity of O^{2-} ions. We already reported the potential–pO^{2-} diagram for the Al–Ca–O–Cl system at 1123 K as a part of the study on the electrochemical reduction of borosilicate glass whose components were SiO_2, B_2O_3, Na_2O, K_2O, and Al_2O_3.[20] In the present study, we update the diagram in which the Ca content in liquid Al is newly considered. Second, cyclic voltammetry is conducted to investigate the reduction behavior of Al_2O_3, whereby the electrode potential is accurately controlled and measured with a three-electrode system by using a Ag^+/Ag reference electrode.[10] Third, Al_2O_3 powder and Al_2O_3 tubes are electrolytically reduced by potentiostatic electrolysis using Fe box-type and Mo box-type electrodes. Finally, based on the results of analyzing the products and the potential–pO^{2-} diagrams, the reaction mechanisms of the electrochemical reduction of Al_2O_3 tube and powder are discussed.

Experimental

A schematic drawing of the experimental apparatus for molten $CaCl_2$ is shown in Fig. 2. In an open dry chamber (dew point $< -65\,^{\circ}C$, HRW-60AR, Daikin Co. Ltd.), 350 g of $CaCl_2$ (> 95.0%, Wako Pure Chemical Industries, Ltd.) was crushed and put in an alumina crucible (purity 99%, o.d.: 90 mm, height: 140 mm, As One Corp.). Then, the crucible containing $CaCl_2$ was dried at 453 K in a vacuum oven for more than 72 h. It was transferred to a stainless steel inner vessel settled in a Kanthal vessel, and vacuumed at 773 K for 24 h to further remove residual moisture. The experiments were conducted inside the Kanthal vessel at 1123 K under a dry Ar atmosphere. A chromel–alumel thermocouple was used for the temperature control. Electrochemical measurements and potentiostatic electrolysis were conducted by a three-electrode method using an electrochemical measurement system (HZ-3000, Hokuto Denko Corp.).

Three types of working electrodes, shown in Fig. 3, were used depending on the purpose. An Al_2O_3-sealed electrode was prepared by inserting a W rod (> 99.95%, diameter: 2.0 mm, Nilaco Corp.) in an Al_2O_3 tube (99.6%, o.d.: 3.0 mm, i.d.: 2.0 mm, Nikkato Corp.), as shown in Fig. 3a. An Fe box-type electrode (6 mm × 6 mm × 10 mm) was prepared with an Fe sheet (99.5%, thickness: 0.10 mm, Nilaco Corp.). After spot-welding of a Mo wire current lead (Fig. 3b), approximately 100 mg of Al_2O_3 powder (99.9%, particle size: 0.212–0.5 mm, Kojundo Chemical Lab. Corp.) was charged in the Fe box-type electrode. A Mo box-type electrode (12 mm × 12 mm × 3 mm), shown in Fig. 3c, was fabricated from a Mo sheet (99.5%, thickness: 0.10 mm, Nilaco Corp.), for which small Fe sheets used to reinforce the corners of the box. The Mo box-type electrode was used for the reduction of an Al_2O_3 tube (99.6%, o.d.: 10 mm, i.d.: 6 mm, Nikkato Corp.). The counter electrode was a square rod of graphite (5 mm × 5 mm × 50 mm, IG-110, Toyo Tanso Co., Ltd.), and the reference electrode was a Ag^+/Ag electrode.[10]

After the potentiostatic electrolysis, the Al_2O_3-sealed electrodes were rinsed with distilled water to remove the residual salts and dried at room temperature. Then, they were cut by a desktop abrasive cutting machine (RC-120, As One Corp.) into sections of approximate length 10 mm. The samples prepared with Fe-box and Mo-box electrodes were washed with anhydrous ethylene glycol (99.5%, Wako Pure Chemical Industries Ltd.) using an ultrasonic washing machine and rinsed with anhydrous acetone (99.5%, Wako Pure Chemical Industries Ltd.). Ethylene glycol was used because it dissolves $CaCl_2$ without reacting with Ca alloy. X-ray diffractometry (XRD; Rigaku, Ultima IV, Cu-$K\alpha$ ray, $\lambda = 1.5418$ Å, 40 kV, 40 mA) was used for sample identification. The samples were observed by using an optical digital microscope (Dino Lite PRO Polarizer DILITE30 AM-413ZT, Sanko Co., Ltd.) and scanning electron microscopy (SEM; VE-8800, Keyence Corp.). The elemental composition of the sample surfaces was analyzed by energy-dispersive X-ray spectroscopy (EDX; EDAX Genesis APEX2, AMETEK Co., Ltd., accelerating voltage: 15 kV). The aluminum droplets obtained by the electrolysis were dissolved into 0.528 mL of 30 wt% HCl solution. Then, pure water was added to a total volume of 50 mL. Inductively coupled plasma atomic emission spectrometry (ICP-AES; SPECTRO Blue, Hitachi High-Tech Science Group) was used for the elemental analysis.

Potential–pO^{2-} Diagrams in Molten $CaCl_2$ at 1123 K

The electrode potential and the activity of O^{2-} ions in the electrolyte are two major factors that determine the electrochemical

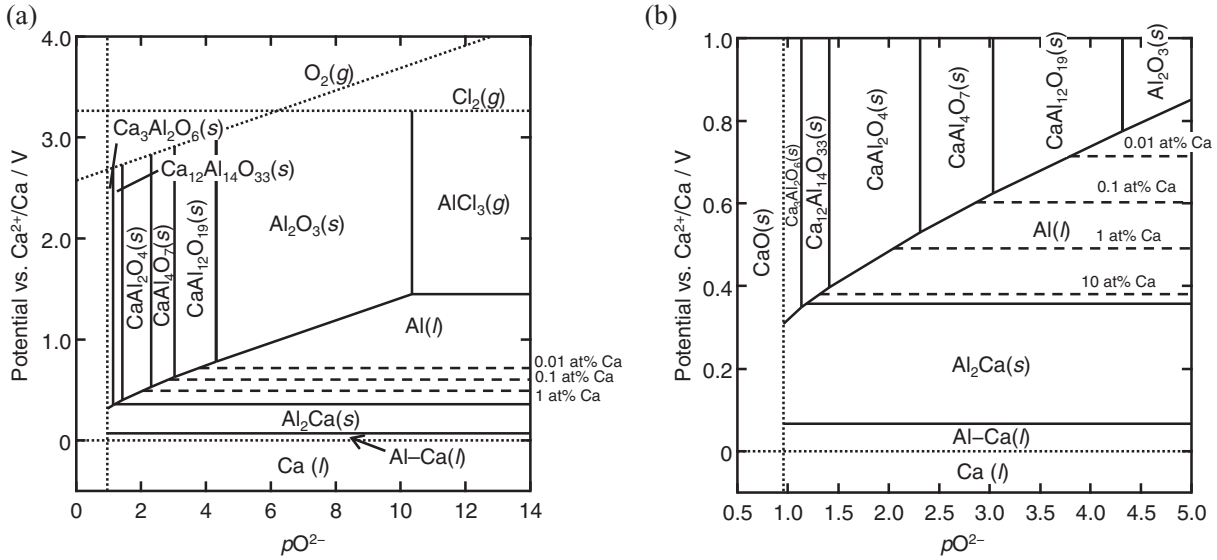

Figure 4. Potential–pO^{2-} diagrams for the Al–Ca–O–Cl system in molten $CaCl_2$ at 1123 K for the (a) whole region and (b) low-pO^{2-} region.

reduction of oxides in molten salts. In several previous studies on the electrochemical reduction of solid oxides in molten salts, potential–pO^{2-} diagrams have been used to thermodynamically predict the chemical and electrochemical behaviors of the substances. A potential–pO^{2-} diagram was first applied to the electrowinning process by Littlewood.[21] Potential–pO^{2-} diagrams have been reported for TiO_2 in molten $CaCl_2$,[22–25] $NiTiO_3$ in $CaCl_2$,[26] SiO_2 in $CaCl_2$,[10,20] Al_2O_3 in $CaCl_2$-based molten salts,[15,20] and for many other substances in various molten salts.[27–35] Yan and Fray constructed potential–pO^{2-} diagrams for the Al–Ca–O–Cl system in molten NaCl–$CaCl_2$ and LiCl–$CaCl_2$,[15] and reported that the experimental results for the electrolytic reduction of Al_2O_3 were consistent with the predictions.

In the present study, potential–pO^{2-} diagrams for the Al–Ca–O–Cl system in molten $CaCl_2$ at 1123 K are created, as shown in Fig. 4, to predict suitable conditions for the production of Al metal and to interpret the electrolysis results. Fig. 4a depicts the diagram with wide potential and wide pO^{2-} regions ($-0.5\ V < E < +4.0$ V vs. Ca^{2+}/Ca, $0 < pO^{2-} < 14$). To discuss the reduction of Al_2O_3, Fig. 4b focuses on the negative-potential and low-pO^{2-} regions ($-0.1\ V < E < +1.0$ V, $0.5 < pO^{2-} < 5.0$). The dotted lines indicate the frame of the potential–pO^{2-} diagram for $CaCl_2$ at 1123 K, i.e., deposition of Ca metal, evolution of Cl_2 and O_2 gases, and precipitation of solid CaO.

Table I. Thermochemical data for the Al–Ca–O–Cl system at 1123 K.

Compound	Phase	Standard Gibbs energy of formation/kJ mol^{-1}	References
$CaCl_2$	Liquid	−629.6	36
CaO	Solid	−517.4	36
CaO	Liquid	−496.9	10
Al_2O_3	Solid	−1320.2	37,38
$AlCl_3$	Gas	−525.6	36
Al_2Ca	Solid	−65.1	39
*$CaAl_{12}O_{19}$	Solid	−8510.7	36,40–42
$CaAl_2O_4$	Solid	−1879.1	43–45
$CaAl_4O_7$	Solid	−3211.7	36,40–42
$Ca_3Al_2O_6$	Solid	−2926.0	40–42
$Ca_{12}Al_{14}O_{33}$	Solid	−15790.2	43

*$CaAl_{12}O_{19}$ was not considered in our previous research.[20] Potential–pO^{2-} diagrams for the Al–Ca–O–Cl system in Ref. 20 were updated as those in Fig. 4.

Table I lists the thermochemical data used for the construction of the diagrams.[36–45] The diagrams in Fig. 4 are essentially similar to that reported in our previous study.[20] As for the differences, the detailed information on alloy formation and Ca content in the liquid phase has been added. Furthermore, the stable region for $CaAl_{12}O_{19}$ has appeared in the present version.

According to the phase diagram of the binary Al–Ca system,[39] as shown in Fig. 5, the stable phases at 1123 K are Al-rich Al–Ca liquid alloy, solid Al_2Ca, and Ca-rich Al–Ca liquid alloy. Here, the Ca content, x_{Ca}, in the Al-rich Al–Ca liquid alloy that equilibrates with Al_2Ca is 0.16. Because the activity of Ca was reported to be 1.7×10^{-3} at this composition at 1373 K,[46] the activity coefficient, γ_{Ca}, and electrode potential, E, in the {Al-rich Al–Ca (l) and Al_2Ca (s)} two-phase state at 1123 K are calculated to be:

$$\gamma_{Ca}\,(x_{Ca} = 0.16) = 3.85 \times 10^{-3} \quad [3]$$

$$E\,(\text{Al-rich Al}-\text{Ca}\ \ (l)\,/\text{Al}_2\text{Ca}\,(s)) = 0.357\,\text{V vs. Ca}^{2+}/\text{Ca} \quad [4]$$

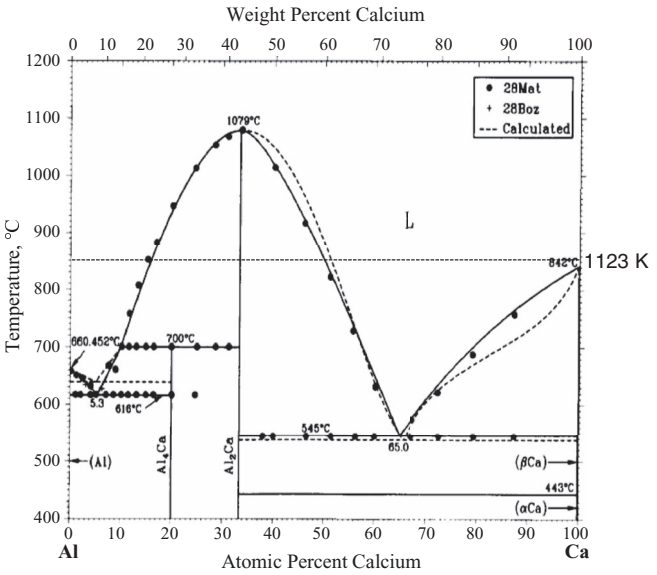

Figure 5. Phase diagram for the Al–Ca system.[39]

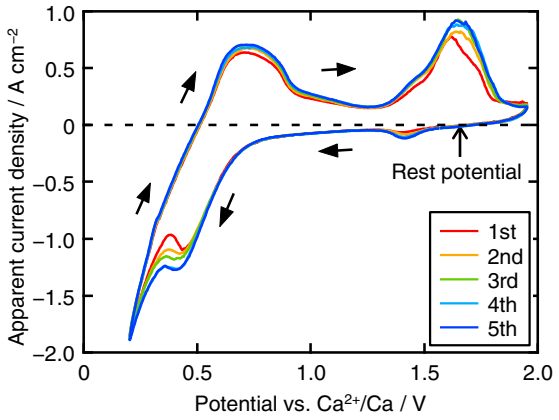

Figure 6. Cyclic voltammograms for an Al_2O_3-sealed electrode in molten $CaCl_2$ at 1123 K. Scan rate: 50 mVs^{-1}. Switching potential: 0.20 V.

Here, the interaction parameter, Ω, is assumed to be independent of temperature ($\Omega = RT \ln \gamma = const. \therefore T \ln \gamma = const.$), where R and T are the gas constant and the absolute temperature, respectively. In the same manner, the electrode potential in the {Ca-rich Al–Ca (l) and Al_2Ca (s)} two-phase state at 1123 K is estimated from the reported activity of Ca, 0.313, at 1619 K.[47]

$$E\,(\text{Ca-rich-Al}-\text{Ca}\,(l)\,/\text{Al}_2\text{Ca}\,(s)) = 0.067\ \text{V vs. Ca}^{2+}/\text{Ca} \qquad [5]$$

Based on the above calculations, the stable regions in the potential–pO^{2-} diagram are determined for Al-rich Al–Ca alloy (l), Al_2Ca (s), and Ca-rich Al–Ca alloy (l). There is a wide stable region of liquid Al in the high-pO^{2-} region, i.e., low activity of O^{2-} ions. Here, the content of Ca in the liquid Al is determined by the electrode potential. The potential values corresponding to several representative Ca contents in the liquid Al are plotted with dashed lines in Figs. 4a and 4b. Al_2Ca is predicted to be formed at potentials more negative than 0.36 V. Ca-rich Al–Ca(l) alloy forms at potentials more negative than 0.067 V. When the thermodynamic data obtained by FP-CALPHAD method[48] is adopted, the potentials of Al_2Ca formation and Ca-rich Al–Ca(l) alloy formation are calculated as 0.310 V and 0.101 V, respectively. The potential at the three-phase equilibrium between $CaAl_{12}O_{19}$, Al, and Al_2O_3 is 0.78 V, $pO^{2-} = 4.31$. A total of five stable regions for calcium aluminates appear in the low-pO^{2-} range: $CaAl_{12}O_{19}$ ($3.04 \le pO^{2-} \le 4.31$, $E \ge 0.62$ V), $CaAl_4O_7$ ($2.31 \le pO^{2-} \le 3.04$, $E \ge 0.53$ V), $CaAl_2O_4$ ($1.41 \le pO^{2-} \le 2.31$, $E \ge 0.40$ V), $CaAl_4O_7$ ($1.16 \le pO^{2-} \le 1.41$, $E \ge 0.35$ V), and $Ca_{12}Al_{14}O_{33}$ ($1.08 \le pO^{2-} \le 1.16$, $E \ge 0.34$ V). It should be noted that $Ca_{12}Al_{14}O_{33}$ did not appear in the Al–Ca–O phase diagram at 1273 K published in 1990,[49] because its thermodynamic data was reported recently.

Results and Discussion

Cyclic voltammetry.—The reduction behavior of Al_2O_3 in the three-phase zone is investigated by cyclic voltammetry using an Al_2O_3-sealed electrode. Fig. 6 shows cyclic voltammograms (CVs) measured in a potential range of 0.2–1.9 V (vs. Ca^{2+}/Ca) for five consecutive cycles. The apparent current density is calculated by using the cross-sectional area of the W rod (dia. 2 mm). In the first cycle, when the scan starts from the rest potential (ca. 1.7 V) in the negative direction, the reduction current sharply increases from 0.6 V and gives a peak at ca. 0.45 V. According to the potential–pO^{2-} diagram (Fig. 4), the reaction is expected to be the electrochemical reduction of Al_2O_3 to Al metal:

$$\text{Al}_2\text{O}_3 + 6\,\text{e}^- \rightarrow 2\text{Al}\,(l) + 3\,\text{O}^{2-} \qquad [6]$$

The cathodic current further increases from 0.35 V, which would correspond to the formation of Al_2Ca:

$$2\,\text{Al} + \text{Ca}^{2+} + 2\,\text{e}^- \rightarrow \text{Al}_2\text{Ca}\,(s) \qquad [7]$$

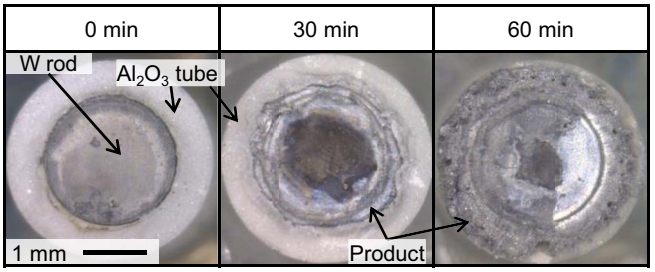

Figure 7. Microscope images of the Al_2O_3 sealed electrodes before and after the potentiostatic electrolysis at 0.30 V for 0, 30, and 60 min in molten $CaCl_2$ at 1123 K.

In addition, the current increases with the cycle number, which indicates an increase in the effective reaction zone of conductor/Al_2O_3/molten salt by the formation of conductive products, such as metallic Al and Al_2Ca.

Potentiostatic electrolysis of Al_2O_3-sealed electrodes.—The reduction of Al_2O_3 is investigated by potentiostatic electrolysis of Al_2O_3-sealed electrodes at 0.30 V for 30 and 60 min. Microscope images of the samples before and after electrolysis are shown in Fig. 7. After 30 min, there are traces of reduction at the Al_2O_3 tube near the W rod. In the case of 60 min, the traces of reduction have spread in the outer direction. These results indicate that the reduction starts in the three-phase zone of Al_2O_3, the conductive W rod, and molten $CaCl_2$. From an EDX analysis of the 60-min sample, the composition of the reacted area is O 20 at%, Al 60 at %, which confirms the electrochemical reduction of Al_2O_3.

Potentiostatic electrolysis of Al_2O_3 powder using Fe box-type electrodes.—With reference to the CV results, potentiostatic electrolysis of Al_2O_3 powder is conducted at 0.50, 0.40, 0.30, 0.25, and 0.20 V for 6 h using Fe-box electrodes to investigate the potential dependence of reaction. Fig. 8a shows the current–time curves during the electrolysis. Larger cathodic currents are observed at more negative potentials. Cross-sectional optical images of the obtained samples are shown in Fig. 8b. The powders are found at the bottom and the solidified $CaCl_2$ are found above the powders in the Fe-box electrodes. The color of the powder changes from white to black at 0.40 V, to greenish-brown at 0.30 V and 0.25 V, and to metallic silver at 0.20 V.

XRD patterns of the powders are shown in Fig. 9. The distinct peak pattern for $Ca_{12}Al_{14}O_{33}$ is observed for the samples at 0.25, 0.30, 0.40, and 0.50 V. Yan and Fray also reported that $Ca_{12}Al_{14}O_{33}$ was formed in the electrochemical reduction of Al_2O_3 in $CaCl_2$-based melt.[15] The patterns for 0.30, 0.40, and 0.50 V indicate the existence of unreacted Al_2O_3, where the peak intensities are smaller at more negative potentials. For the sample at 0.20 V, only the Al_2Ca phase is confirmed. Incidentally, the inner surface of the Fe-box electrode had changed to Al_5Fe_2 (PDF # 00-047-1435) after electrolysis of Al_2O_3 powder at 0.4 V for 12 h, which is confirmed by its appearance and XRD analysis (Fig. 10). Since the Fe-box alloyed with the produced Al, the Al_5Fe_2 formed at the surface. The more internal parts of Fe walls may have contained other Al–Fe alloy phases with higher Fe content. However, they could not be detected by XRD due to the limited penetration depth of X-ray.

$Ca_{12}Al_{14}O_{33}$ has been reported to form free electrons in the cage framework of a crystal structure by a deoxidation reaction, showing a green color owing to the transition of free electrons to the conduction band and metallic conductivity at room temperature.[50–54] The samples obtained at 0.25 and 0.30 V, which are composed of $Ca_{12}Al_{14}O_{33}$, exhibit a greenish color, suggesting that they have high conductivity after the electrochemical deoxidation. After Al_2O_3 powder in an Fe-box electrode is immersed in $CaCl_2$ for 6 h without electrolysis, the formation of $Ca_{12}Al_{14}O_{33}$ is not confirmed. Thus, the $Ca_{12}Al_{14}O_{33}$ at

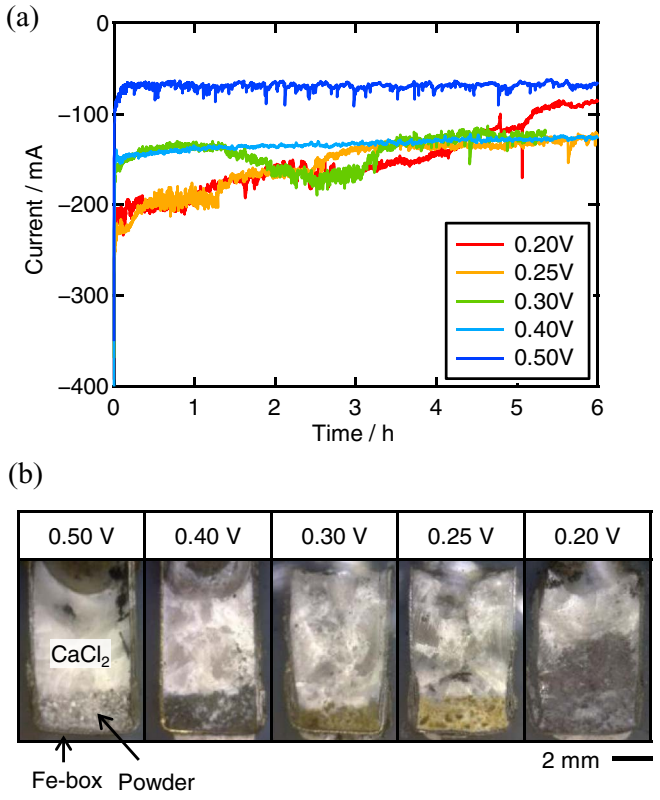

Figure 8. (a) Current–time curves during the potentiostatic electrolysis of the Fe-box electrodes containing Al_2O_3 powder at 0.50, 0.40, 0.30, 0.25, and 0.20 V for 6 h in molten $CaCl_2$ at 1123 K. (b) Cross-sectional optical images of the samples obtained by the potentiostatic electrolysis.

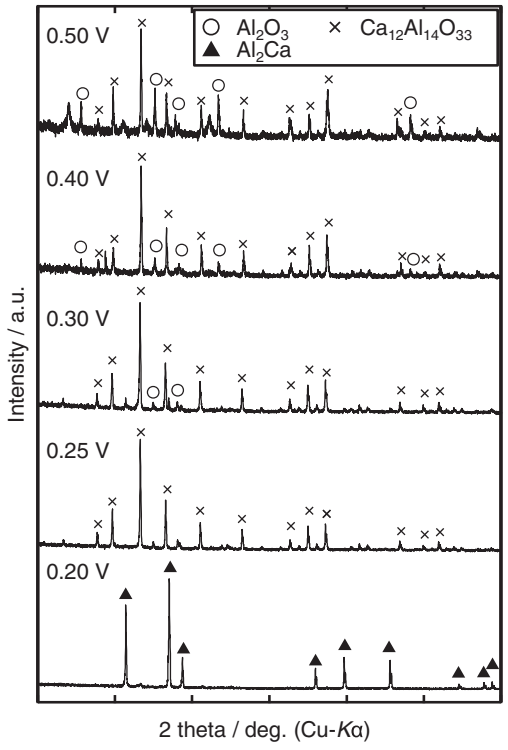

Figure 9. XRD patterns of the samples obtained by the potentiostatic electrolysis of Al_2O_3 powder in the Fe-box electrodes at 0.50, 0.40, 0.30, 0.25, and 0.20 V for 6 h in molten $CaCl_2$ at 1123 K.

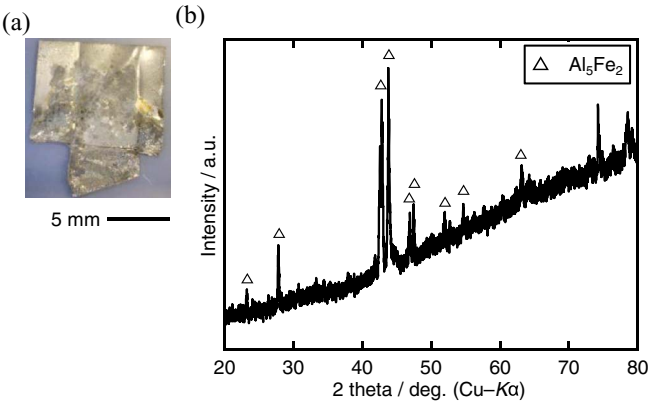

Figure 10. (a) Optical image and (b) XRD pattern of the Fe-box electrode after the potentiostatic electrolysis of Al_2O_3 powder at 0.40 V for 12 h in molten $CaCl_2$ at 1123 K.

0.25 and 0.30 V is considered to be formed by the reaction of Al_2O_3, Ca^{2+}, and electrochemically formed O^{2-} ions.

To summarize these results, the mechanism of the reduction of Al_2O_3 powder in an Fe-box electrode is described as follows.

(1) At first, Al_2O_3 in contact with the Fe-box electrode is reduced to Al_5Fe_2 alloy.

$$5\,Al_2O_3 + 4\,Fe + 30\,e^- \rightarrow 2\,Al_5Fe_2 + 15\,O^{2-} \quad [8]$$

(2) In the vicinity of the reduced Al_2O_3 powder, $Ca_{12}Al_{14}O_{33}$ is formed by the reaction of Al_2O_3, Ca^{2+}, and the electrochemically produced O^{2-} ions.

$$12\,Ca^{2+} + 12\,O^{2-} + 7Al_2O_3 \rightarrow Ca_{12}Al_{14}O_{33} \quad [9]$$

(3) The $Ca_{12}Al_{14}O_{33}$ near the Fe-box electrode is reduced to form Al_5Fe_2 alloy.

$$5\ Ca_{12}Al_{14}O_{33} + 28\,Fe + 210\,e^- \rightarrow 14\,Al_5Fe_2 + 60\,Ca^{2+} + 165\,O^{2-} \quad [10]$$

(4) When the electrode potential is below 0.20 V, $Ca_{12}Al_{14}O_{33}$ is electrochemically reduced to form Al_2Ca.

$$Ca_{12}Al_{14}O_{33} + 56\,e^- \rightarrow 7Al_2Ca + 5\,Ca^{2+} + 33\,O^{2-} \quad [11]$$

Considering that the obtained phases are $Ca_{12}Al_{14}O_{33}$ and Al_2Ca alloy for the Fe-box electrodes, the concentration of O^{2-} ions in the three-phase zone of Al_2O_3/molten salt/conductor is high ($pO^{2-} < 1.41$) during the electrolysis. The high concentration of O^{2-} ions is believed to be brought about by the stagnation of O^{2-} ions in the Al_2O_3 powder. The diffusion of O^{2-} ions from the electrochemical reaction interface to the bulk molten salt is not easy, owing to the long diffusion paths passing through the gaps between the Al_2O_3 particles. In order to obtain Al metal with low Ca content, the concentration of O^{2-} ions must be kept low ($pO^{2-} > 2.86$ for Ca content < 0.1 at%) To realize this, the diffusion of O^{2-} ions from the reaction interface to the bulk molten salt has to be facile. For this purpose, a new electrode structure, in which a dense Al_2O_3 tube is placed on a flat metal plate, is considered to be effective.

Potentiostatic electrolysis of Al_2O_3 tube in a Mo box-type electrode.—On the basis of the above considerations, the electrochemical reduction of Al_2O_3 tube is carried out using a Mo-box electrode with a wide bottom and a shallow depth (Fig. 3c). Mo has been used instead of Fe, because it is not easily alloyed with Al.

Fig. 11 shows a current–time curve during the potentiostatic electrolysis at 0.25 V for 12 h. A nearly constant current of −200 mA is observed. Fig. 12a shows an optical image of the sample after the electrolysis. Black products are found around the Al_2O_3 tube. After

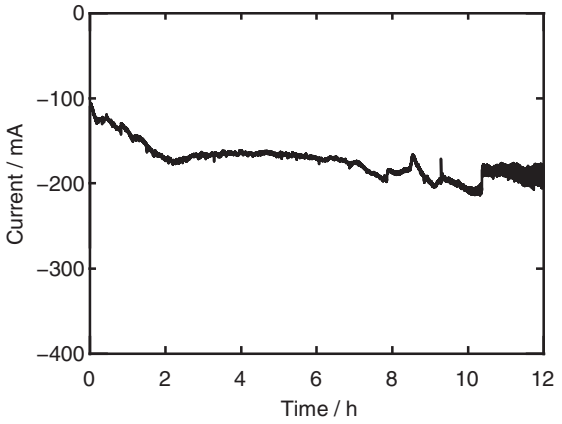

Figure 11. A current–time curve during the potentiostatic electrolysis of Al_2O_3 tube in the Mo-box electrode at 0.25 V for 12 h in molten $CaCl_2$ at 1123 K.

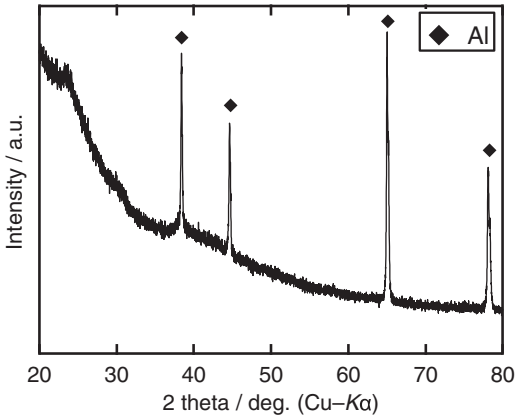

Figure 13. XRD pattern of the metal droplets obtained from the bottom of the crucible after potentiostatic electrolysis of the Al_2O_3 tube in the Mo-box electrode at 0.25 V for 12 h in molten $CaCl_2$ at 1123 K.

washing the sample with ethylene glycol (Fig. 12b), evident decreases in height and wall thickness are observed for the Al_2O_3 tube. Moreover, metallic droplets with an approximate maximum diameter of 3 mm are obtained from the bottom of the crucible (Fig. 12c). The total mass of the droplets is 32 mg. Fig. 13 shows an XRD pattern of the droplets, which confirms the formation of Al metal. An ICP-AES analysis of the obtained Al droplets reveals that the composition is 95.4–98.0 at% Al and 2.0 at%–4.5 at% Fe. The concentrations of Ca and Mo are less than the detection limit. In this experiment, the level of detection limit for ICP-AES is 1–2 × 10^{-2} at %. The current efficiency is calculated to be approximately 50% from the mass loss of the Al_2O_3 tube, 605 mg, and the charge during the electrolysis, 3431 C. The background current of the Mo-box electrode is likely the main reason for the low efficiency. In addition, formation of dissolved Ca in molten $CaCl_2$, which induces shuttle current between the anode and the cathode, is another cause of the low current efficiency; the solubility of metallic Ca in molten $CaCl_2$ is reported to be ca. 3 mol% at 1123 K.[55] The black deposits in the Mo-box electrode are identified as Al_2Ca by XRD analysis. The Al_2Ca phase is considered to be precipitated from liquid Al–Ca alloy upon cooling.

The above results have demonstrated that the new electrode structure is effective. Fig. 14 compares the diffusion paths of O^{2-} ions for

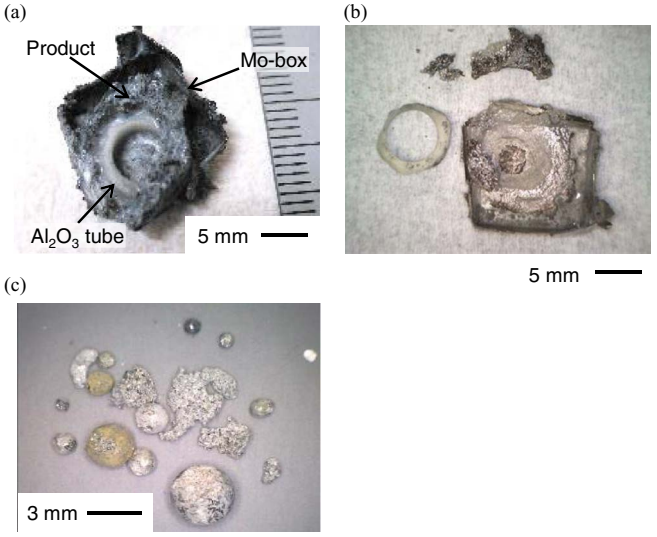

Figure 12. Optical images after the potentiostatic electrolysis of the Al_2O_3 tube in the Mo-box electrode at 0.25 V for 12 h in molten $CaCl_2$ at 1123 K (a) before and (b) after washing the Mo-box electrode, and (c) metal droplets obtained from the bottom of the crucible after the electrolysis.

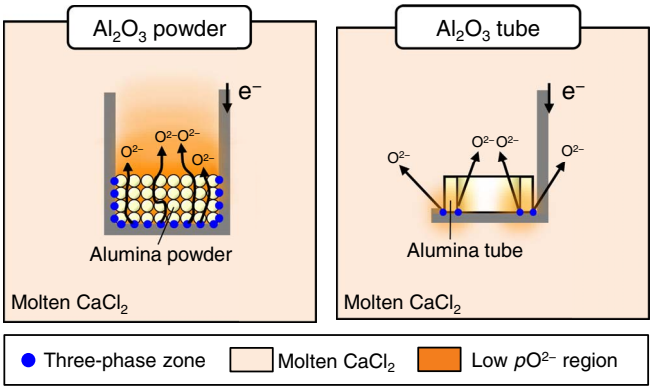

Figure 14. Difference in diffusion paths between the electrolysis of Al_2O_3 powder and tube.

Al_2O_3 powder and Al_2O_3 tube. Electrochemical reduction of Al_2O_3 occurs at the three-phase zone to produce O^{2-} ions, which decrease the value of pO^{2-}. In the case of powder, the diffusion of O^{2-} ions is slow due to the small space among particles (left in Fig. 14), which causes the very low pO^{2-} in the three-phase zone. The deeper color means the low pO^{2-} region, i.e., the high O^{2-} ion concentration region. On the contrary, for the tube, the facile diffusion of O^{2-} ions enables the higher pO^{2-} in the three-phase zone. According to the potential–pO^{2-} diagram, the production of Al metal is possible only when the pO^{2-} is not very low. Thus, even for Al_2O_3 powder, the production of Al metal is expected by using a larger particle size and/or by performing agitation.

Conclusions

The electrochemical reduction of solid Al_2O_3 has been investigated in molten $CaCl_2$ at 1123 K. Cyclic voltammetry using an Al_2O_3-sealed electrode indicates that the reduction of Al_2O_3 proceeds at potentials more negative than 0.6 V. When Al_2O_3 powder is electrolyzed in an Fe-box electrode, $Ca_{12}Al_{14}O_{33}$ is formed at 0.25 and 0.30 V, and Al_2Ca is formed at 0.20 V. However, Al droplets are obtained from the bottom of a crucible by the electrolysis of an Al_2O_3 tube in a Mo-box electrode at 0.25 V. The difference in the reduction behavior is explained by the diffusivity of O^{2-} ions from the reaction interface to the bulk molten salt and thermodynamic considerations using the potential–pO^{2-} diagrams.

ORCID

Toshiyuki Nohira https://orcid.org/0000-0002-4053-554X

References

1. G. Z. Chen, D. J. Fray, and T. W. Farthing, *Nature*, **407**, 361 (2000).
2. D. J. Fray, *JOM*, **53**, 27 (2001).
3. G. Z. Chen, D. J. Fray, and T. W. Farthing, *Metall. Mater. Trans. B Process Metall. Mater. Process. Sci.*, **32**, 1041 (2001).
4. R. L. Centeno-Sánchez, D. J. Fray, and G. Z. Chen, *J. Mater. Sci.*, **42**, 7494 (2007).
5. A. M. Abdelkader, K. T. Kilby, A. Cox, and D. J. Fray, *Chem. Rev.*, **113**, 2863 (2013).
6. W. Xiao and D. Wang, *Chem. Soc. Rev.*, **43**, 3215 (2014).
7. T. Nohira, K. Yasuda, and Y. Ito, *Nat. Mater.*, **2**, 397 (2003).
8. X. Jin, P. Gao, D. Wang, X. Hu, and G. Z. Chen, *Angew. Chem.*, **43**, 733 (2004).
9. W. Xiao, X. Jin, Y. Deng, D. Wang, X. Hu, and G. Z. Chen, *ChemPhysChem*, **7**, 1750 (2006).
10. K. Yasuda, T. Nohira, R. Hagiwara, and Y. H. Ogata, *J. Electrochem. Soc.*, **154**, E95 (2007).
11. W. Xiao, X. Jin, and G. Z. Chen, *J. Mater. Chem. A*, **1**, 10243 (2013).
12. X. Yang, K. Yasuda, T. Nohira, R. Hagiwara, and T. Homma, *J. Electrochem. Soc.*, **161**, D3116 (2014).
13. X. Y. Yan, *Metall. Mater. Trans. B Process Metall. Mater. Process. Sci.*, **39**, 348 (2008).
14. H. Xie, H. Zhang, Y. Zhai, J. Wang, and C. Li, *J. Mater. Sci. Technol.*, **25**, 459 (2009).
15. X. Y. Yan and D. J. Fray, *J. Appl. Electrochem.*, **39**, 1349 (2009).
16. H. Xie, J. Wang, Y. Zhai, X. Hu, and C. Li, *The Open Materials Science Journal*, **5**, 83, (2011).
17. A. V. Suzdaltsev, A. P. Khramov, Y. P. Zaikov, A. A. Pankratov, E. G. Vovkotrub, and B. D. Antonov, *J. Electrochem. Soc.*, **164**, H5183 (2017).
18. D. A. Wenz, I. Johnson, and R. D. Wolson, *J. Chem. Eng. Data*, **14**, 250 (1969).
19. J. J. Brennan and J. A. Pask, *J. Am. Ceram. Soc.*, **51**, 569 (1968).
20. Y. Katasho, K. Yasuda, and T. Nohira, *J. Electrochem. Soc.*, **164**, D478 (2017).
21. R. Littlewood, *J. Electrochem. Soc.*, **109**, 525 (1962).
22. K. Dring, R. Dashwood, and D. Inman, *J. Electrochem. Soc.*, **152**, D184 (2005).
23. K. Dring, R. Dashwood, and D. Inman, *J. Electrochem. Soc.*, **152**, E104 (2005).
24. K. Dring, R. Bhagat, M. Jackson, R. Dashwood, and D. Inman, *J. Alloys Compd.*, **419**, 103 (2006).
25. R. Bhagat, D. Dye, S. L. Raghunathan, R. J. Talling, D. Inman, B. K. Jackson, K. K. Rao, and R. J. Dashwood, *Acta Mater*, **58**, 5057 (2010).
26. B. K. Jackson, D. Dye, D. Inman, R. Bhagat, R. J. Talling, S. L. Raghunathan, M. Jackson, and R. J. Dashwood, *J. Electrochem. Soc.*, **157**, E57 (2010).
27. M. Takahashi, Y. Katsuyama, and Y. Kanzaki, *J. Electroanal. Chem. Interfacial Electrochem.*, **62**, 363 (1975).
28. G. Picard, F. Seon, and B. Tremillon, *J. Electrochem. Soc.*, **129**, 1450 (1982).
29. R. Lysy and G. Duyckaerts, *Anal. Chim. Acta*, **96**, 125 (1978).
30. G. Landresse and G. Duyckaerts, *Anal. Chim. Acta*, **73**, 121 (1974).
31. L. D. Brown, R. Abdulaziz, R. Jervis, V. J. Bharath, R. C. Attwood, C. Reinhard, L. D. Connor, S. J. R. Simons, D. Inman, D. J. L. Brett, and P. R. Shearing, *J. Nucl. Mater.*, **464**, 256 (2015).
32. A. M. MartıÍnez, Y. Castrillejo, E. Barrado, G. M. Haarberg, and G. Picard, *J. Electroanal. Chem.*, **449**, 67 (1998).
33. D. Lambertin, J. Lacquement, S. Sanchez, and G. Picard, *Electrochem. Commun.*, **4**, 447 (2002).
34. Y. Ito, H. Hayashi, Y. Itoh, and S. Yoshizawa, *Bull. Chem. Soc. Jpn.*, **58**, 3172 (1985).
35. H. Hayashi, S. Yoshizawa, and Y. Ito, *Electrochim. Acta*, **28**, 149 (1983).
36. Landolt-Börnstein, *Thermodynamic Properties of Inorganic Material, Scientific Group Thermodata Europe (SGTE)*, Springer-Verlag, Berlin-Heidelberg, (1999).
37. I. Barin, O. Knacke, and O. Kubaschewski, *Thermochemical Properties of Inorganic Substances, Supplement*, Springer-Verlag, Berlin, (1977).
38. I. Barin, O. Knacke, and O. Kubaschewski, *Thermochemical Properties of Inorganic Substances, Supplement*, Springer-Verlag, Berlin and New York, (1977).
39. V. P. Itkin, C. B. Alcock, P. J. van Ekeren, and H. A. J. Oonk, *J. Phase Equilib.*, **9**, 652 (1988).
40. I. Barin, *Thermochemical Data of Pure Substances, Part I*, VCH Verlags Gesellschaft, Weinheim, (1993).
41. I. Barin, *Thermochemical Data of Pure Substances, Part II*, VCH Verlags Gesellschaft, Weinheim, (1993).
42. A. J. Bard, R. Parsons, and J. Jordan, *Standard potentials in aqueous solution*, Marcel Dekker Inc., New York, (1985).
43. I. Barin, *Thermochemical Data of Pure Substances*, VCH Verlags Gesellschaft, Weinheim, (1989).
44. O. Knacke, O. Kubaschewski, and K. Hesselman, *Thermochemical Properties of Inorganic Substances*, 2nd ed., Springer-Verlag, Berlin, (1991).
45. M. Binnewies and E. Milke, *Thermochemical Data of Elements and Compounds*, 2nd edition, Wiley-VCH, Weinheim, (2002).
46. K. T. Jacob, S. Srikanth, and Y. Waseda, *Trans. Jpn. Inst. Met.*, **29**, 50 (1988).
47. E. Schürmann, P. Fünders, and H. Litterscheidt, *Archiv für das Eisenhüttenwesen*, **46**, 473 (1975).
48. K. Ozturk, Y. Zhong, L. Q. Chen, Z. K. Liu, J. O. Sofo, and C. Wolverton, *Metall. Mater. Trans. A*, **36**, 5 (2005).
49. R. O. Suzuki, M. Ikezawa, T. H. Okabe, T. Oishi, and K. Ono, *Mater. Trans. JIM*, **31**, 61 (1990).
50. S. Kim, M. Miyakawa, K. Hayashi, T. Sakai, M. Hirano, and H. Hosono, *J. Am. Chem. Soc.*, **127**, 1370 (2005).
51. S. W. Kim, Y. Toda, K. Hayashi, M. Hirano, and H. Hosono, *Chem. Mater.*, **18**, 1938 (2006).
52. S. W. Kim, K. Hayashi, M. Hirano, H. Hosono, and I. Tanaka, *J. Am. Ceram. Soc.*, **89**, 3294 (2006).
53. S. Matsuishi, Y. Toda, M. Miyakawa, K. Hayashi, T. Kamiya, M. Hirano, I. Tanaka, and H. Hosono, *Science*, **301**, 626 (2003).
54. S. W. Kim, S. Matsuishi, T. Nomura, Y. Kubota, M. Takata, K. Hayashi, T. Kamiya, M. Hirano, and H. Hosono, *Nano Lett*, **7**, 1138 (2007).
55. R. A. Sharma, *J. Phys. Chem.*, **74**, 3896 (1970).